Statistical mechanics of helical wormlike chain model

Ya Liu, Toni Pérez, Wei Li, J. D. Gunton, and Amanda Green

Citation: J. Chem. Phys. **134**, 065107 (2011); doi: 10.1063/1.3548885
View online: http://dx.doi.org/10.1063/1.3548885
View Table of Contents: http://jcp.aip.org/resource/1/JCPSA6/v134/i6
Published by the American Institute of Physics.

Statistical mechanics of helical wormlike chain model

Ya Liu,[1,a)] Toni Pérez,[1] Wei Li,[1] J. D. Gunton,[1] and Amanda Green[2]
[1]*Department of Physics, Lehigh University, Bethlehem, Pennsylvania 18015, USA*
[2]*Department of Physics, Bucknell University, Lewisburg, Pennsylvania 17837, USA*

(Received 3 November 2010; accepted 4 January 2011; published online 14 February 2011)

We investigate the statistical mechanics of polymers with bending and torsional elasticity described by the helical wormlike model. Noticing that the energy function is factorizable, we provide a numerical method to solve the model using a transfer matrix formulation. The tangent–tangent and binormal–binormal correlation functions have been calculated and displayed rich profiles which are sensitive to the combination of the temperature and the equilibrium torsion. Their behaviors indicate that there is no finite temperature Lifshitz point between the disordered and helical phases. The asymptotic behavior at low temperature has been investigated theoretically and the predictions fit the numerical results very well. Our analysis could be used to understand the statics of dsDNA and other chiral polymers. © *2011 American Institute of Physics*. [doi:10.1063/1.3548885]

I. INTRODUCTION

The statistical mechanics of DNA and other semiflexible (wormlike) chains has received considerable attention in recent literature. A variety of models have been proposed to predict the behavior of semiflexible chains and to explain experimental results. Among these models, the freely jointed chain[1] and the Kratky–Porod wormlike chain model[2–4] have been widely used to describe intrinsically straight polymer molecules. Other models that have been used to describe the coupling of DNA stiffness parameters include the Marko–Siggia[5] and the revised Marko–Siggia[6] models. Since bending and torsional elasticities are crucial in determining the static and dynamic properties of biopolymers such as dsDNA and sickle hemoglobin (HbS),[7–9] many models have been suggested based on the linear polymer.[10–14] As a natural extension of the wormlike model, the helical wormlike model is one of the simplest models which leads to a helix structure at zero temperature.[14,15] In addition, a recent model of developable ribbons has been proposed to describe the statistical mechanical properties of ribbonlike objects.[16]

In this paper we present the results of a statistical mechanics theory of the helical wormlike chain model. It is motivated by a desire to understand the structural properties of biopolymers, such as dsDNA and sickle hemoglobin polymer bundles,[17] and their dependence on temperature and equilibrium torsions, as characterized by the behavior of various correlation functions for the chain (e.g., the tangent–tangent and binormal–binormal correlation functions). The equilibrium torsion of polymers is quite variable and is an important control parameter in our model. For example, dsDNA has a radius of about 1.1 nm and a pitch of approximately 34 nm, which corresponds to an equilibrium torsion of approximately 0.17. The typical sickle hemoglobin bundle is thought to consist of 14 intertwined helical strands (paired into seven double strands) and has a radius of approximately 11 nm and a pitch of about 270 nm, corresponding to a torsion of about 0.02. These represent rather different limits of the helical wormlike chain model, as we will show in subsequent sections. Recently, simulation and experimental studies of the torsional stiffness of DNA have been carried out,[18,19] further indicating the importance of studying the effects of torsion in models of biopolymers. Our study involves a formulation of the model in terms of a transfer matrix, as formulated by Quine *et al.*[13] and Giomi and Mahadavan.[16] Since the Hamiltonian is factorizable, we are able to obtain a numerical solution using the transfer matrix. We have calculated the tangent–tangent and binormal–binormal correlation functions, which characterize the structure of the model and depend on physical parameters that enter the Hamiltonian (the bending and torsion constants), as well as on the temperature and equilibrium torsion. We find that these correlation functions display a rather rich behavior, which corresponds to different equilibrium structures of the model. This behavior is sensitive to the combination of the temperature and the equilibrium torsion. In the low temperature limit we show that the behavior of these correlation functions can be described rather accurately by a perfect helical structure, whose radius and pitch length change with the equilibrium torsion. The correlation functions thus display a pure oscillatory behavior in the zero-temperature limit. At finite temperatures this helical structure persists only over a finite length scale, so the correlation functions display a damped oscillatory behavior. These oscillations are damped out due to the effects of thermal energy. We also find that the tangent–tangent correlation function has a damped, oscillatory behavior at all temperatures; hence there is no finite temperature at which there is a transition to a purely damped behavior. Thus the oscillatory behavior of the tangent–tangent correlation function implies that there is an underlying helical structure that persists at any finite temperature. Therefore there is no finite temperature critical point ("Lifshitz point")[20,21] that divides the helical and disordered phases for this model. A similar result was found in a study of the statistical mechanics

a)Author to whom correspondence should be addressed. Electronic mail: yal209@lehigh.edu.

of developable ribbons,[16] a model which has no spontaneous twist.

The outline of the paper is as follows. In Sec. II we define the model and formulate its solution in terms of a transfer matrix. In Sec. III we present a numerical solution of the model as a function of the temperature and equilibrium torsion that enters the Hamiltonian. In Sec. IV we present a low temperature theoretical analysis and in Sec. V we present a brief conclusion.

II. HELICAL WORMLIKE CHAIN MODEL

Since bending and torsional elasticities are crucial in determining the static and dynamic properties of biopolymers, such as dsDNA and sickle hemoglobin, many models have been suggested based on the linear polymer model.[10,11,13,14] The helical wormlike model is a simple model leading to helical structure at zero temperature.[14,15] The energy for this model is given as

$$H = \frac{\kappa_b}{2}\int_0^L \kappa^2\, ds + \frac{\kappa_\tau}{2}\int_0^L (\tau-\tau_0)^2\, ds, \tag{1}$$

where κ is the curvature, τ is the torsion, L is the polymer length, and τ_0 is the equilibrium torsion. κ_b, κ_τ are the bending and torsional stiffness, respectively. The geometrical information of the linear chain is fully described in terms of the Frenet frame,[10,22] in which three orthogonal unit vectors form a moving trihedron, namely, tangent (**t**), normal (**n**), and binomal (**b**) vectors (Fig. 1). Therefore, $\kappa = |\frac{\partial \mathbf{t}(s)}{\partial s}|$ and $\tau = \pm|\frac{\partial \mathbf{b}(s)}{\partial s}|$ (+: right-handed chirality; –: left-handed chiraliy). Since the helical wormlike model was proposed, many studies of it have been made using methods such as Green's function and Wiener integral formulations.[11,14] Though the energy form [Eq. (1)] favors $\tau = \tau_0$, an ambiguity in the torsion in this model arises at $\kappa = 0$ since in this case, **n** and **b** are not well-defined. Other models have been proposed to couple τ and κ to avoid this ambiguity.[10] Nevertheless, the helical wormlike model has been widely used to model the covalent bonding interactions for the protein structure determination due to its simplicity. Here we provide a numerical method to explore the properties of the model.

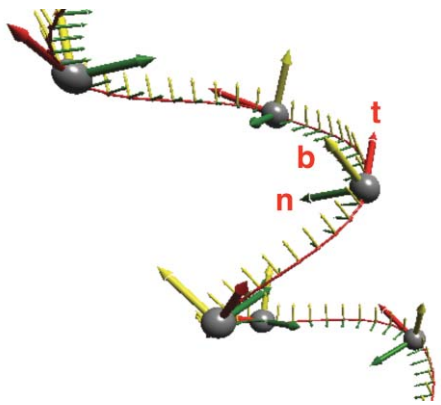

FIG. 1. Frenet frame describing (**t**,**n**,**b**) along a chain.

One can discretize the polymer chain by joining $N = L/a$ consecutive segments with bond length a. At each vertex, the local Frenet frame $(\mathbf{t}_i, \mathbf{n}_i, \mathbf{b}_i)$ is constructed by using the relations

$$\mathbf{t}_i = \frac{\mathbf{r}_{i+1}-\mathbf{r}_i}{a}, \mathbf{b}_i = \frac{\mathbf{t}_{i-1}\times\mathbf{t}_i}{|\mathbf{t}_{i-1}\times\mathbf{t}_i|}, \mathbf{n}_i = \mathbf{b}_i\times\mathbf{t}_i, \tag{2}$$

where $\mathbf{r}_i$ is the position vector and $s \Leftrightarrow ia, \mathbf{f}(s) \Leftrightarrow \mathbf{f}_i$, and $\frac{\partial \mathbf{f}(s)}{\partial s} \Leftrightarrow a^{-1}(\mathbf{f}_i - \mathbf{f}_{i-1})$. We use a discretization of H that is given as follows:

$$H = \frac{\kappa_b a^{-1}}{2}\sum_{i=1}^{N}(\mathbf{t}_i - \mathbf{t}_{i-1})^2 + \frac{\kappa_\tau a^{-1}}{2}\sum_{i=1}^{N}(\pm\sqrt{(\mathbf{b}_i - \mathbf{b}_{i-1})^2} - \tau_0)^2, \tag{3}$$

where we introduce $\cos\theta_i = \mathbf{t}_i\cdot\mathbf{t}_{i-1}$, and $\cos\phi_i = \mathbf{b}_i\cdot\mathbf{b}_{i-1}$. In this version of the discretization [Eq. (2)], $\mathbf{b}_i\cdot\mathbf{t}_{i-1} = 0$, $\mathbf{b}_i\cdot\mathbf{t}_i = 0$. Thus one can overlap the ith and $(i-1)$th frames by two consecutive rotations: first, rotate about $\mathbf{t}_{i-1}$ by the angle ϕ_i, such that $\mathbf{b}_{i-1}$ and $\mathbf{b}_i$ collapse; second, rotate about $\mathbf{b}_i$ by the angle θ_i so that two frames overlap. The local Frenet frames are therefore related through the rotation matrix $(\mathbf{t}_i, \mathbf{n}_i, \mathbf{b}_i) = (\mathbf{t}_{i-1}, \mathbf{n}_{i-1}, \mathbf{b}_{i-1})\mathbf{R}_{i-1}$, where $\mathbf{R}_i$ is the transfer matrix obtained from the multiplication of the two rotations explained above,

$$\mathbf{R}_i = \begin{pmatrix} \cos\theta_i & -\sin\theta_i & 0 \\ \sin\theta_i\cos\phi_i & \cos\theta_i\cos\phi_i & -\sin\phi_i \\ \sin\theta_i\sin\phi_i & \cos\theta_i\sin\phi_i & \cos\phi_i \end{pmatrix}. \tag{4}$$

Thus,

$$(\mathbf{t}_N, \mathbf{n}_N, \mathbf{b}_N) = (\mathbf{t}_0, \mathbf{n}_0, \mathbf{b}_0)\mathbf{R}_0\mathbf{R}_1\cdots\mathbf{R}_{N-1}. \tag{5}$$

Notice that $\mathbf{t}_i\cdot\mathbf{n}_{i-1} = \sin\theta_i\cos\phi_i$ and $\mathbf{t}_i\cdot\mathbf{b}_{i-1} = \sin\theta_i\sin\phi_i$; θ_i and ϕ_i are also the polar and azimuthal angles in the spherical coordinate of the ith Frenet frame, which simplifies H to

$$H = \sum_{i=0}^{N}\kappa_b a^{-1}(1-\cos\theta_i) + 2\kappa_\tau a^{-1}\left(\sin\frac{\phi_i}{2} - \frac{\tau_0}{2}\right)^2, \tag{6}$$

with $\theta_i \in (0,\pi)$, $\phi_i \in (-\pi,\pi)$. The signs $\pm$ before the torsion disappear, since they have been incorporated in the expression of H [Eq. (6)]. The partition function can be calculated by

$$Z = \int e^{-\beta H}\prod_{i=1}^{N} d\theta_i d\phi_i = z_1^N, \tag{7}$$

$$z_1 = \int e^{-\beta\left[\kappa_b(1-\cos\theta)+2\kappa_\tau(\sin\frac{\phi}{2}-\frac{\tau_0}{2})^2\right]}\sin\theta\, d\theta d\phi, \tag{8}$$

where we use the fact that the energy factorizes and $\beta = \frac{1}{k_b T}$, and from now on all the lengths are measured in the unit of a. Introducing the statistical average $\langle A\rangle = \frac{1}{Z}\mathrm{Tr}(Ae^{-\beta H})$, since $\langle\mathbf{R}_0\mathbf{R}_1\cdots\mathbf{R}_{N-1}\rangle = \langle\mathbf{R}\rangle^N$, one can get

$$\langle\mathbf{t}_N\cdot\mathbf{t}_0\rangle = \left(\langle\mathbf{R}\rangle^N\right)_{11}, \tag{9}$$

$$\langle\mathbf{b}_N\cdot\mathbf{b}_0\rangle = \left(\langle\mathbf{R}\rangle^N\right)_{33}, \tag{10}$$

which provides us a numerical method to calculate the correlation functions.

III. THEORY AND NUMERICAL RESULTS

Since the correlation functions can be determined from the transfer matrix through Eqs. (9) and (10), we use linear algebra to analyze the matrix. The eigenvalues of $\langle \mathbf{R} \rangle$ are determined by the roots of the characteristic polynomial : $|\langle \mathbf{R} \rangle - \lambda I| = 0$, where $|\mathbf{M}|$ stands for the determinant of a matrix $\mathbf{M}$. Generally, if the discriminant of a real matrix is nonpositive (for example, the rotation matrix), the three roots or the eigenvalues can be written as

$$\lambda_1 = ae^{ib}, \lambda_2 = ae^{-ib} \text{ and } \lambda_3 = c, \tag{11}$$

where a, b, and c are the real functions of the four averages defined as $\langle \cos\theta \rangle = ct$, $\langle \sin\theta \rangle = st$, $\langle \cos\phi \rangle = cp$, $\langle \sin\phi \rangle = sp$. A matrix $\mathbf{V}$ whose columns are the eigenvectors of $\langle \mathbf{R} \rangle$ will diagonalize it through a similarity transformation, with

$$\langle \mathbf{R} \rangle^N = \mathbf{V}^{-1} \begin{pmatrix} \lambda_1^N & & \\ & \lambda_2^N & \\ & & \lambda_3^N \end{pmatrix} \mathbf{V}.$$

The elements of $\langle \mathbf{R} \rangle^N$ are the linear combination of λ_1^N, λ_2^N, and λ_3^N; the correlation functions can be written as

$$\langle \mathbf{t}_N \cdot \mathbf{t}_0 \rangle = A_t e^{-\frac{N}{l_1}} + B_t e^{-\frac{N}{l_2}} \cos(kN), \tag{12}$$

$$\langle \mathbf{b}_N \cdot \mathbf{b}_0 \rangle = A_b e^{-\frac{N}{l_1}} + B_b e^{-\frac{N}{l_2}} \cos(kN), \tag{13}$$

where A_t, B_t, A_b, and B_b are independent of N and determined by $\mathbf{V}$. They satisfy the relations

$$A_t + B_t = 1, A_b + B_b = 1. \tag{14}$$

k is the wavenumber and l_1, l_2 are the persistence lengths, respectively, given by

$$l_1^{-1} = -\ln c, l_2^{-1} = -\ln a, \tag{15}$$

$$k = b. \tag{16}$$

κ_b and κ_τ are related through the Poisson ratio[23] σ: $\kappa_b = \kappa_\tau(1+\sigma)$. These persistence lengths reflect the effect of thermal energy in damping out the ground-state helical structure and depend on the physical stiffness parameters of the model, as well as temperature. The Poisson ratio for isotropic material in elasticity theory is limited to $\sigma \in (-1, 0.5)$. In our numerical solution, κ_b is set equal to κ_τ as an illustration, which is compatible with the case of dsDNA whose $\kappa_b \approx 50\,\text{nm}, \kappa_\tau \approx$ 30–50 nm (Ref. 19). Defining $\alpha = \beta\kappa_b = \beta\kappa_\tau$, the temperature varies in the range so that $\alpha \in (10, 1000)$, which covers the well-known values of many biopolymers such as dsDNA and HbS. The characteristic torsions of dsDNA and a sickle hemoglobin bundle are 0.17 and 0.02, respectively. Unfortunately, the Poisson ratio for sickle hemoglobin falls outside the range of our analysis, since it is approximately 50 (Ref. 24). In our following analysis, we investigate the behavior of the correlation functions for both small equilibrium torsion values, $\tau_0 = 0.02$ and 0.2, and large torsion $\tau_0 = 0.9$. We will present in Sec. IV, an analysis of the asymptotic behavior in the low temperature limit that explains many of the results which we now show.

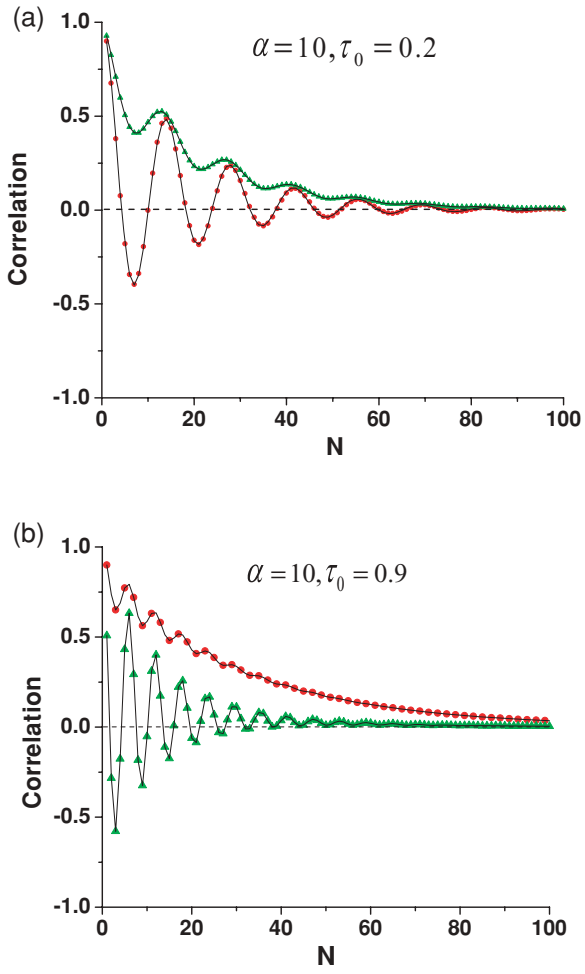

FIG. 2. Tangent (circles) and binormal (triangles) correlation functions for two different values of the torsional angle τ_0 obtained by numerical evaluation of Eqs. (9) and (10), respectively. The temperature was kept fixed to $\alpha = 10$. Solid lines correspond to a fitting using Eqs. (12) and (13), respectively.

Figure 2 shows how the tangent and binormal correlation functions change for different values of τ_0. We observe an exponential decay together with a periodic oscillation of the binormal correlation function, while the tangent correlation function exhibits exponentially damped oscillations for a value of the torsional angle close to that observed in DNA. For higher values of τ_0, we observe a crossover between the behavior of these two correlation functions, as shown in Fig. 2. It is also worth noting that the wavenumber k increases as τ_0 increases. We can also explore the effect that the temperature has on the correlation functions. Figure 3 illustrates the behavior of the correlation functions at low temperature. We can still see the crossover in the behavior of the correlation functions as τ_0 increases, but now the exponential decay is less accentuated.

We can use Eqs. (12) and (13) to fit the tangent and binormal correlation function data obtained previously from numerical evaluation of the exact analytical expressions. The result of the fitting is indicated with solid lines in Figs. 2 and 3.

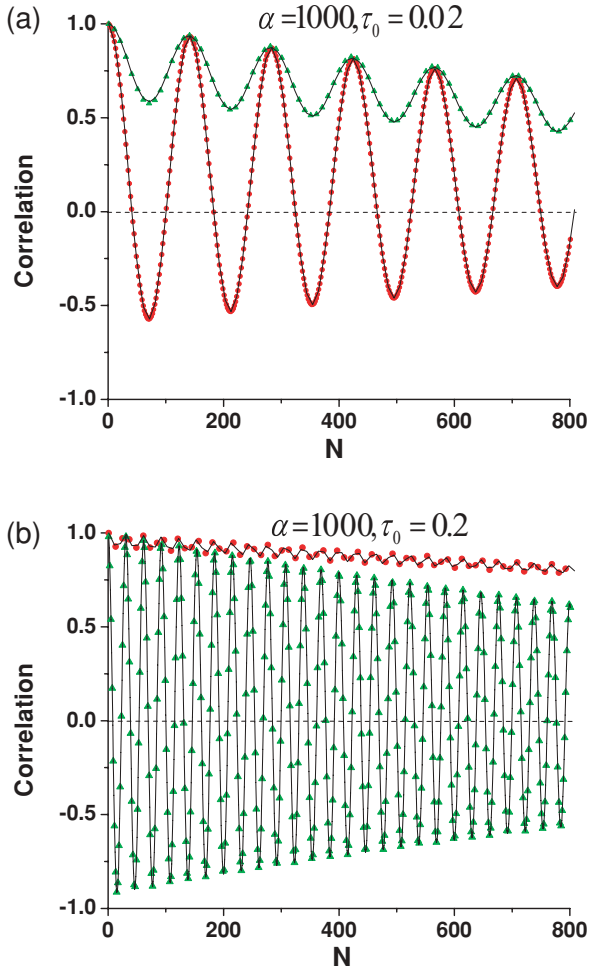

FIG. 3. Tangent (circles) and binormal (triangles) correlation functions for different τ_0 obtained by numerical evaluation of Eqs. (9) and (10), respectively. The temperature is $\alpha = 1000$. Solid lines correspond to a fitting using Eqs. (12) and (13).

A rather accurate agreement is found in all the cases that we studied.

The persistence lengths l_1 and l_2, together with the wavenumber k associated with the periodic oscillations, also have a remarkable dependence on the torsion angle τ_0. In Fig. 4 we show how l_2 increases as the the torsion increases, reaching a saturation for larger values of τ_0. In contrast, l_1 slightly decreases as the torsion increases. The wavenumber satisfies a linear dependence on the torsion angle τ_0. In Fig. 5 we determine the dependence of the wavenumber with temperature for different τ_0 values.

Finally, in Fig. 6, we illustrate that both bending and twisting persistence lengths are linear functions of temperature. As the temperature decreases, we expect that the decay lengths in Eqs. (12) and (13) increase, with the structure becoming more like that of the perfect helical structure expected at zero temperature. This helix can be defined using the following parameterization in Cartesian coordinates:

$$x = r\cos t,\ y = r\sin t,\ z = \frac{p}{2\pi}t, \tag{17}$$

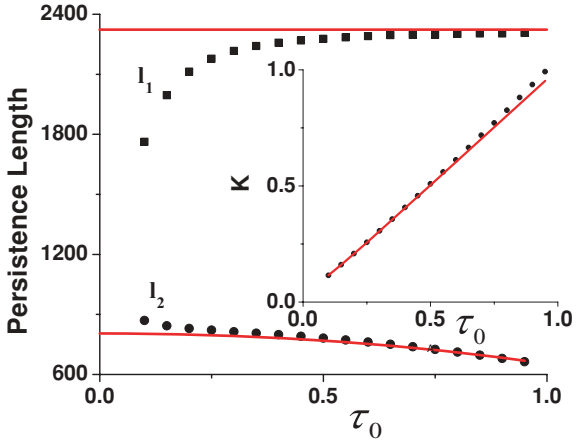

FIG. 4. Torsional dependence of the persistence length parameters l_1 (squares) and l_2 (circles). Solid lines are the prediction given by Eqs. (28) and (29), respectively. Inset: Wavenumber as a function of τ_0. Solid lines correspond to theoretical calculation given by Eq. (27). Other parameters: $\alpha = 500$.

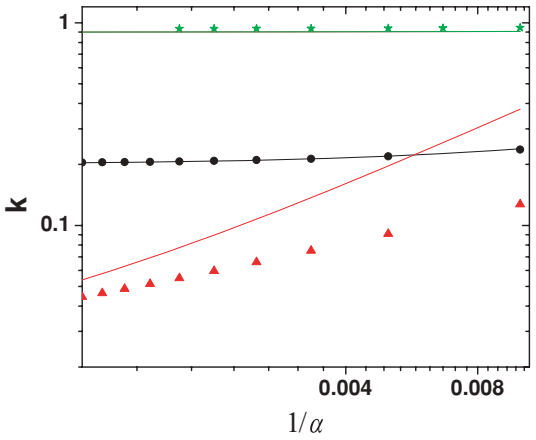

FIG. 5. Temperature dependence of the wavenumber for different τ_0. From bottom to top, $\tau_0 = 0.02$, 0.2, and 0.9. Lines represent the theoretical prediction given by Eq. (27).

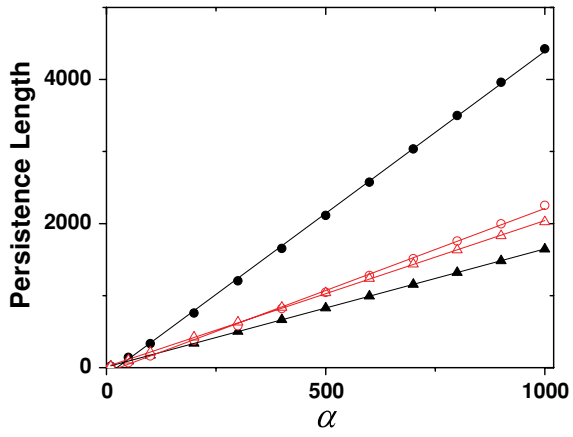

FIG. 6. Temperature dependence of the persistence length l_1 (circles) and l_2 (triangles) for different values of the torsional angle: $\tau_0 = 0.2$ (filled symbols) and $\tau_0 = 0.02$ (open symbols). Lines represent the theoretical prediction given by Eqs. (28) and (29), respectively.

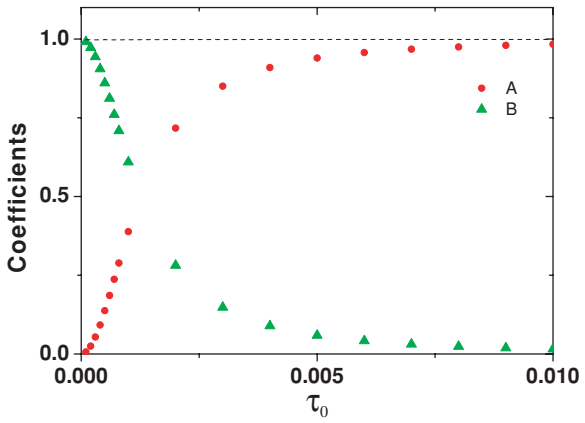

FIG. 7. Plot of τ_0 dependence of the coefficients, A (circles) and B (triangles) for $\alpha = 10^6$. Dashed line indicates the summation of A and B in agreement with the theoretical prediction.

where r is the radius and p is the pitch. The correlation functions therefore are characterized by r and p

$$\langle \mathbf{t}(s) \cdot \mathbf{t}(0) \rangle = A + B \cos\left(\frac{s}{\sqrt{r^2 + (\frac{p}{2\pi})^2}} \right), \tag{18}$$

$$\langle \mathbf{b}(s) \cdot \mathbf{b}(0) \rangle = B + A \cos\left(\frac{s}{\sqrt{r^2 + (\frac{p}{2\pi})^2}} \right), \tag{19}$$

where $A = \frac{r^2}{r^2+(\frac{p}{2\pi})^2}$, $B = \frac{(\frac{p}{2\pi})^2}{r^2+(\frac{p}{2\pi})^2}$, and $A + B = 1$. We confirm the helical ground-state by studying the case of $\alpha = 10^6$ numerically, and fitting the correlation functions using Eqs. (18) and (19). Figure 7 indicates that the results are in the agreement with the theoretical predictions.

IV. ASYMPTOTIC BEHAVIOR IN THE LOW TEMPERATURE LIMIT

Since the typical values of the persistence lengths of ds-DNA and HbS are large in comparison with the bond length, in this section we focus on obtaining an approximate theoretical description of the low temperature limit, $\beta \to \infty$, of the correlation functions, for equilibrium torsion angles greater than zero. In order to understand the behavior of those correlation functions, we evaluate the eigenvalues of the transfer matrix $\langle \mathbf{R} \rangle$ using Eq. (8) and find that two of the elements can be evaluated exactly,

$$ct = \coth(\beta\kappa_b) - \frac{1}{\beta\kappa_b}, \tag{20}$$

$$st = \frac{\pi}{2} I_1(\beta\kappa_b)\mathrm{csch}(\beta\kappa_b), \tag{21}$$

where $I_n(x)$ is the modified Bessel function of the first kind. In the limit as $\beta \to \infty$, these reduce to

$$st \approx \sqrt{\frac{\pi}{2\beta\kappa_b}}, ct \approx 1 - \frac{1}{\beta\kappa_b}. \tag{22}$$

In this low temperature limit we can use a steepest descent approximation to calculate the remaining elements. Namely, the ϕ part of the integral of partition function [Eq. (8)] can be approximated as

$$\int_{-\pi}^{\pi} e^{-2\beta\kappa_\tau(\sin\frac{\phi}{2} - \frac{\tau_0}{2})^2} d\phi \approx 2\int_{-\frac{\pi}{2}}^{\frac{\pi}{2}} e^{-2\beta\tilde{\kappa}_\tau(\phi - \sin^{-1}\frac{\tau_0}{2})^2} d\phi$$
$$= \sqrt{\frac{\pi}{2\beta\tilde{\kappa}_\tau}} \left[\mathrm{erf}\left(\sqrt{2\beta\tilde{\kappa}_\tau} \left(\frac{\pi}{2} - \sin^{-1}\tau_0 \right) \right) \right.$$
$$\left. + \mathrm{erf}\left(\sqrt{2\beta\tilde{\kappa}_\tau} \left(\frac{\pi}{2} + \sin^{-1}\tau_0 \right) \right) \right], \tag{23}$$

where $\tilde{\kappa}_\tau = \kappa_\tau(1 - \frac{\tau_0^2}{4})$ and erf$[x]$ is the error function.

We do a similar approximation for the averages of sp and cp and find their asymptotic behavior (to order of $\frac{1}{\beta}$) is given by

$$sp \approx \tau_0\sqrt{1 - \frac{\tau_0^2}{4}}, cp \approx \left(1 - \frac{\tau_0^2}{2}\right)\left(1 - \frac{1}{2\beta\tilde{\kappa}_\tau}\right). \tag{24}$$

Using the average of Eq. (4) and introducing $\rho = 1 - \frac{\tau_0^2}{2}$, the transfer matrix thus has the following form to order $\frac{1}{\beta}$ and τ_0^2:

$$\begin{pmatrix} 1 - \frac{1}{\beta\kappa_b} & -\sqrt{\frac{\pi}{2\beta\kappa_b}} & 0 \\ \rho\sqrt{\frac{\pi}{2\beta\kappa_b}} & \rho\left(1 - \frac{1}{\beta\kappa_b} - \frac{1}{2\beta\tilde{\kappa}_\tau}\right) & -\tau_0 \\ \tau_0\sqrt{\frac{\pi}{2\beta\kappa_b}} & \tau_0\left(1 - \frac{1}{\beta\kappa_b}\right) & \rho(1 - \frac{1}{2\beta\tilde{\kappa}_\tau}) \end{pmatrix}. \tag{25}$$

We note that the approximations made in Eq. (25) ignore terms of order $\beta^{-3/2}$, therefore our approximation requires

$$\beta\tau_0 \gg 1. \tag{26}$$

Using the matrix [Eq. (25)] and Eq. (16), we obtain the wavenumber

$$k \approx \tau_0 + \frac{\pi}{4\tau_0\beta\kappa_b} + \left(\frac{1}{2\beta\tilde{\kappa}_\tau} - \frac{\pi}{32\beta\kappa_b}\right)\tau_0. \tag{27}$$

Note that k asymptotically approaches the equilibrium value of torsion τ_0 in this low temperature limit. In Fig. 4, we show that the numerical results are consistent with Eq. (27), as illustrated by the solid curve in the inset. The dependence of k on $\frac{1}{\beta}$ is also illustrated in Fig. 5 for $\tau_0 = 0.02, 0.2,$ and 0.9. The difference between the theoretical predictions and numerical data is significant in the case of $\tau_0 = 0.02$ due to the breakdown of the condition [Eq. (26)]. The persistence length l_1 satisfies

$$l_1^{-1} \approx (1 - \frac{\pi}{4})\frac{1}{\beta\kappa_b}, \tag{28}$$

which is only a function of the (bare) bending stiffness constant and is independent of τ_0. Figure 4 shows the agreement between our predictions and our numerical results for relatively large τ_0. The discrepancy in the regime of small τ_0 we

believe is due to the breakdown of the condition given by Eq. (26). The persistence length l_2 satisfies

$$l_2^{-1} \approx \frac{1-\pi/4}{\beta\kappa_b} + \frac{1}{2\beta\tilde{\kappa}_\tau}, \tag{29}$$

which is also illustrated in Fig. 4. The linear dependence of l_1, l_2 on $\frac{1}{\beta}$ is also observed in Fig. 6 for $\tau_0 = 0.02$ and 0.2.

V. CONCLUSION

We have investigated the helical wormlike model that describes a polymer with both bending and torsional elastic energy. We calculate the tangent–tangent and binormal–binormal correlation functions by a numerical method for different temperatures in two regimes: (i) small equilibrium torsion (τ_0) with the values corresponding to the dsDNA and sickle hemoglobin bundle and (ii) large equilibrium torsion. These show significant differences from the wormlike polymer model, which has no oscillatory behavior. The low temperature asymptotic behavior of the correlation functions has been analyzed using a steepest decent approximation. This gives results that are in good agreement with our numerical calculations, in the region of validity of the approximation. We should also note a difference between our asymptotic results for the persistence length l_2 and that of the ribbon model, for which there is no intrinsic equilibrium torsion. The persistence length l_2 for our model depends on both the bending and (renormalized) torsional stiffness constants, whereas in the ribbon model it depends only on the bending constant. In addition, the asymptotic form of l_1 is only a function of the bending constant, whereas in the ribbon model it is only a function of the torsional stiffness constant.

Finally, we note that our results for the persistence lengths as functions of equilibrium torsion and temperature can be tested, in principle, experimentally. This should help us understand the effects of the intrinsic helicity on the static properties of biopolymers, such as the force–extension relation and torsional–stiffness behavior. In addition, there is a rich area of the dynamical properties of biopolymers that is yet to be fully understood. In this regard, we are currently carrying out Brownian dynamics simulations of the kinetic properties of the helical wormlike chain model.

ACKNOWLEDGMENTS

This work was supported by grants from the Mathers Foundation and the National Science Foundation (Grant DMR-0702890). One of us (A.G.) would like to acknowledge the support of the NSF sponsored Lehigh summer REU program, where her research was conducted.

[1] P. J. Flory, *Statistical Mechanics of Chain Molecules* (Interscience, New York, 1969).
[2] O. Kratky and G. Porod, Recl. Trav. Chim. Pays-Bas. Belg. **69**, 1106 (1949).
[3] H. Daniels, Proc. R. Soc. Edinburgh, Sect. A: Math. Phys. Sci. **63**, 290 (1952).
[4] J. Hermans and R. Ullman, Physica E (Amsterdam) **18**, 951 (1952).
[5] J. Marko and E. Siggia, Macromolecules **27**, 981 (1994).
[6] H. Zhou and Z. Ou-Yang, Phys. Rev. E. **58**, 4816 (1998).
[7] R. E. Goldstein, T. R. Powers, and C. H. Wiggins Phys. Rev. Lett. **80**, 5232 (1998).
[8] I. Klapper and M. Tabor, J. Phys. Math. Gen. **27**, 4919 (1994).
[9] J. D. Moroz and P. Nelson, Macromolecules **31**, 6333 (1998).
[10] R. D. Kamien, Rev. Mod. Phys. **74**, 953 (2002).
[11] K. F. Freed, J. Chem. Phys. **54**, 1453 (1970).
[12] Y. Zhou and G. Chirikjian, J. Chem. Phys. **119**, 4962 (2003).
[13] J. Quine, T. Cross, M. Chapman, and R. Bertram, Bull. Math. Biol. **66**, 1705 (2004).
[14] H. Yamakawa, T. Yoshizaki, and M. Fujii, Macromolecules **10**, 934 (1977).
[15] P. Bugl and S. Fujita, J. Chem. Phys. **50**, 3137 (1969).
[16] L. Giomi and L. Mahadevan, Phys. Rev. Lett. **104**, 238104, (2010).
[17] M. Turner, R. Briehl, F. Ferrone, and R. Josephs, Phys. Rev. Lett. **90**, 128103 (2003).
[18] A. Mazur, Phys. Rev. Lett. **105**, 018102 (2010).
[19] J. Lipfert, J. W. Kerssemakers, T. Jager, and N. Dekker, Nat. Methods **7**, 977 (2010).
[20] S. Redner and H. Stanley, Phys. Rev. B **16**, 4901 (1977).
[21] R. Hornreich, R. Liebmann, H. Schuster, and W. Selke, Z. Phys. B **35**, 91 (1979).
[22] J. R. Weber, BMC Struct. Bio. **9**, 19 (2009).
[23] H. Yamakawa, *Helical Wormlike Chains in Polymer Solutions* (Springer, New York, 1997).
[24] M. Turner, R. Briehl, J. Wang, F. Ferrone, and R. Josephs, J. Mol. Biol. **357**, 1422 (2006).